Title

Shear-Induced Aggregation of Mammalian Synovial Fluid Components under Boundary Lubrication Conditions

Journal

Advanced Functional Materials, 24(21)

ISSN

1616-301X

Authors

Banquy, Xavier
Lee, Dong Woog
Das, Saurabh
et al.

Publication Date

2014-06-01

DOI

10.1002/adfm.201302959

ADVANCED FUNCTIONAL MATERIALS
www.afm-journal.de

Shear-Induced Aggregation of Mammalian Synovial Fluid Components under Boundary Lubrication Conditions

*Xavier Banquy, Dong Woog Lee, Saurabh Das, Jack Hogan, and Jacob N. Israelachvili**

The lubricating and structural properties of different mammalian synovial fluids in thin films undergoing shear between two mica surfaces are studied in detail using a surface force apparatus (SFA). A 10–13 nm thick film of synovial components (proteins, lipids, and polymers) adsorbs on the mica surfaces in less than an hour of incubation time, and induces a strong repulsion between the surfaces that prevents them from coming into contact. Upon shearing, the structure of the confined synovial fluid changes dramatically when sheared above a "critical" shear rate of about 2 s^{-1} (corresponding to approximately 40 nm s^{-1}). Above this critical shear rate and up to at least 70 μm s^{-1}, the proteins and biopolymers in the fluid gradually aggregate to form a homogenous gel layer on each mica surface. As shearing continues, the gel layer gradually breaks up into discrete/individual gel particles that can roll in the contact keeping the sheared surfaces far apart even under high compressive loads (pressure $P \approx 20$ MPa). These particles eventually become elongated and finally behave as roller bearings. This mechanism is consistently observed for three mammalian synovial fluids and two types of surfaces suggesting that it actually occurs in articular joints and prostetic implants in vivo. The implications of these findings for joints and prosthetic implants structure and lubrication are discussed; in particular the formation and function of the *lamina splendens*.

1. Introduction

Even though intense research efforts have been focused on deciphering the molecular mechanism that allows articular joints to support intense stresses and deformations over the life time of a person, it is still unclear what role the synovial fluid (SF) plays under boundary lubrication conditions.

Cartilage surface structures and composition are quite complex and are known to vary from one species to another. Cartilage morphology shows either a columnar structure (fiber-based structure) or leaf-based overall arrangement depending on the species.[1] Besides their differences in structure and composition, articular joints also possess remarkably conserved "ingredients" among mammalian species, which are believed to play a primary role in joint lubrication. Examples of synovial fluid components found in most mammals include (see **Table 1**) hyaluronic acid (HA), the protein PRG4 (also known as lubricin), lipids, seric proteins (mostly albumin and globulin) and glycoaminoglycans (GAGs). These components are produced by either synoviocytes (lining cells of the synovial sac membrane) or by chondrocytes (cells embedded in the cartilage also in charge of producing collagen). Due to its highly porous structure (more than 80% of liquid,[2] cartilage transports large quantities of synovial fluid under transient deformations in and out of its matrix. The cartilage superficial zone (SZ) is also known to be covered by a gel-like layer (*lamina splendens*, LS) containing the same essential components found in the SF, except in much higher concentration.[3] For example, lipids have been found on the SZ at high concentrations and form highly organized structures such as multi-lamellar membrane coatings[4] or even lipid globules.[5] Lubricin is also commonly found at high concentrations at the cartilage surface.[6] The role of the superficial zone in boundary lubrication, and most particularly the LS, is still unclear. However, several reports have shown that partial or total removal of this layer does not affect joint lubrication properties such as wear protection or friction coefficient.[7] This surprising observation raises many fundamental questions on the origin of the LS and its role in maintaining joint protection against wear.

The present study aims to provide answers to these questions, especially concerning the mechanisms at the origin of the formation of the LS and its role in protecting cartilage's fragile surface. For this purpose, we used the surface force apparatus (SFA) to characterize the lubricating properties of synovial fluid from different mammalian species and elucidate the fluid's structural changes under confined shearing conditions.

2. Results and Discussion

Articular joints are complex multi-component systems and therefore difficult to understand or model at the molecular level. Our approach was to simplify the system to a single asperity whose dimensions would be similar to those found in cartilage. Typically, surface asperities in cartilage have a

Prof. X. Banquy,[+] Dr. D. W. Lee, Dr. S. Das, J. Hogan, Prof. J. N. Israelachvili
Chemical Engineering Department
M/C 5080, University of California
Santa Barbara, CA 93106-5080 USA
E-mail: Jacob@engr.ucsb.edu
Tel: 8058938407

[+]Present Address: Faculté de pharmacie, Université de Montréal, Montréal, Québec, Canada H3T 2M4

DOI: 10.1002/adfm.201302959

Table 1. Main components found in human synovial fluid and reported to have a significant impact on the lubricating properties of articular joints.

Component	Concentration in synovial fluid [mg/mL]	Comments
Hyaluronic acid	1–4[8]	The molecular weight of HA is estimated to be 1–6 MDa
Seric proteins	18[9]	11 mg/mL is albumin and 7 mg/mL is γ-globulin
Lubricin	0.05–0.35[10]	20% of the total Lubricin is estimated to be located at the surface of cartilage
Lipids	0.138[11]	45% of the total lipid content is made of DPPC
Glycosaminoglycans	0.15–0.05[12]	Concentration of sulphated glycosaminoglycans.

height of 1–10 μm and a mean distance between asperities from 1–50 μm.[13] Under transient loads, these asperities are expected to have a contact area of 20 to 100 μm in diameter. The geometrical characteristics of a single asperity can easily be attained with the SFA using mica surfaces as model surfaces (**Scheme 1**). One of the advantages of using mica is that, in contrary to the cartilage surface, mica is atomically smooth and non-porous, which reduces the complexity of the system. Therefore, any changes in the interfacial fluid between, rather than within, the surfaces can be accurately observed.

2.1. Normal Interaction Forces Between Mica Surfaces Across Synovial Fluid.

Normal interaction forces between two mica surfaces immersed in human synovial fluid (HSF) are presented in **Figure 1**A. The figure shows the forces on approach as well as on separation of the mica surfaces. Before shearing the surfaces, the measured interaction forces were found to be reversible, meaning that no hysteresis and no adhesion between the surfaces were measured. The interaction force profile, i.e., $F_\perp$ vs D curve, was accurately described by the Alexander–de Gennes (AdG) theory for grafted neutral polymer brushes.[14] The choice of this model rather than more sophisticated charged polyelectrolyte brushes theories was justified by the high salinity of the medium which is expected to screen most of the electrostatic interactions between the polymer chains. The equation describing the interaction forces for such a system is:

$$\frac{F_\perp}{R} = \frac{16\pi kTL_0}{35\sigma^3}\left[7\left(\frac{2L_0}{D}\right)^{5/4} + 5\left(\frac{D}{2L_0}\right)^{7/4} - 12\right] \quad (1)$$

where σ is the average spacing between close neighbor chains and L_0 the equilibrium brush height.

We found that for all the synovial fluids tested, L_0 varied between 60 and 80 nm and σ between 1.1 and 1.2 nm (as discussed later, see **Table 2**). Synovial fluid is a complex mixture of proteins and polyelectrolytes, and it is rather improbable that they would adopt a well defined brush conformation on the mica surface. The observed agreement between our experimental data and the AdG theory suggests that the protein-polyelectrolyte films adsorbed on the surfaces can be described as a purely repulsive effective brush layer. This description still holds after shearing the surfaces for a prolonged time (several hours, see Figure 1A). After shearing, the effective grafting density and brush equilibrium length were systematically much higher. We found that for HSF, L_0 and σ increased to 122 and 0.6 nm after shearing respectively. These results already show that structural changes have occurred in the adsorbed proteous film upon shearing which could be due to accumulation of material in the contact zone or to some more complex structural changes in the molecules constituting the film. As we will show later on, the observed changes in the normal force after shearing involve a very complex transformation in the synovial fluid structure which evolved from an optically and mechanically homogenous fluid to a composite film of protein aggregates and native fluids.

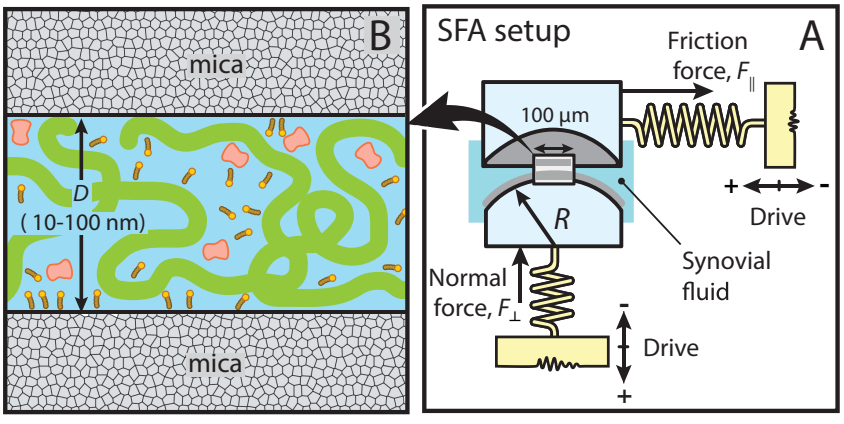

Scheme 1. (A) Mechanical diagram of the SFA for the study of synovial fluid lubrication properties. (B) Cartoon representing the different components of the synovial fluids confined between two mica surfaces.

The general agreement of the AdG theory with the interaction force profiles measured across each tested synovial fluid was confirmed for the three mammal species studied. Figure 1B shows a master curve of all the experimental data collected from human, equine and bovine synovial fluids. The overlapping of all the normalized experimental force curves into a master curve validates the general applicability of the effective brush model for describing adsorbed synovial proteins films.

The applicability of the general brush like behavior to synovial proteins and polymer

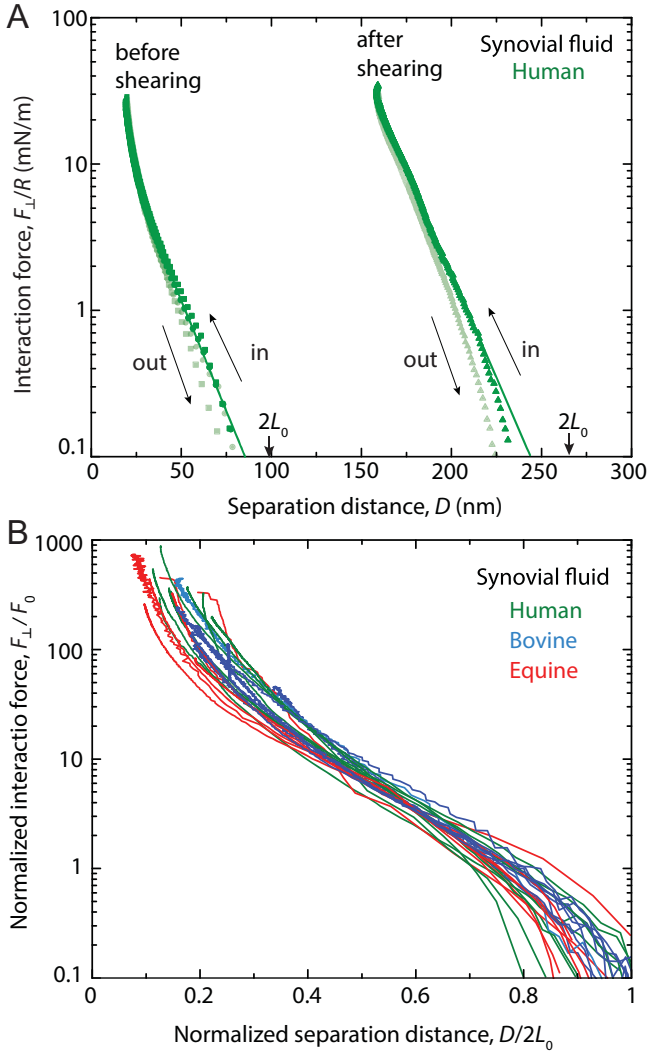

Figure 1. (A) Normal interaction forces between two mica surfaces across human synovial fluid. Before shearing the surfaces the interaction force curve is purely repulsive and show a film thickness at maximum compression of approximately 20 nm. After shearing the surfaces for one hour, the interaction force curve is shifted out with a film thickness at high compression of about 140 nm. (B) Normalized force curves measured before shearing the surfaces for all the synovial fluids tested. The force curves are well described by the AdG theory of end-grafted polymer brushes Equation (1).

films was already suggested by previous studies involving grafted hyaluronic acid,[15] mucin proteins such as lubricin,[16] or GAGs.[17] It is interesting to note that these previous studies have systematically reported a longer range of the interaction forces (starting at around 150 to 200 nm, before shearing) than the one observed in this study (typically below 100 nm) which suggest that protein / polymer films adsorbed from native synovial fluids have a noticeably different structure compared to adsorbed films from reconstituted or model fluids. We recently noticed[18] that grafted HA films tend to collapse upon adsorption of lubricin, which is known to interact strongly with HA.[19] Lubricin was found to physically crosslink the grafted HA layer improving the load carrying capability of the film and also its wear protection properties.[18] These observations suggest that adsorbed films from native synovial fluids should be viewed as highly collapsed films essentially composed of a meshwork of HA and lubricin swelled with synovial fluid.

Table 2. Effective brush thickness L_0 and grafting density s from the AdG brush model Equation (1) used to fit the interaction forces between adsorbed synovial fluid components on mica surfaces.

Animal species	Effective brush thickness, L_0 [nm]	Effective grafting density, σ [nm]
Human	72 ± 15	1.25 ± 0.25
Equine	78 ± 17	1.10 ± 0.22
Bovine	60 ± 13	1.15 ± 0.23

2.2. Application of Shear and Structural Changes of the Confined Synovial Fluid

To further characterize the structural changes of SF under shear, we first confined the fluid between two mica surfaces under a normal load of approximately 0.75 mN ($F_\perp/R$ = 30 mN/m, D = 25 nm), which can be converted to a normal pressure P using the Derjaguin approximation for the crossed cylinders geometry utilized by the SFA:

$$P = -\frac{\partial W}{\partial D} = -\frac{1}{2\pi R}\left(\frac{\partial F_\perp}{\partial D}\right) \quad (2)$$

where W is the interaction energy $W = F_\perp/2\pi R$.

The calculated normal pressure was P = 4.4 MPa. A video recording of the contact zone using normal optical microscopy (top view) was also performed simultaneously to monitor any visual changes in the fluid while shearing. After approaching the surfaces up to a separation distance of D = 25 nm ($F_\perp$ = 0.75 mN, v = 0 nm/s, $F_{//}$ = 0 mN, see **Figure 2**, point a, **Figure 3**A), the upper surface was subjected to a reciprocal sliding motion at v = 2.5 µm/s and an oscillation amplitude of 50 µm peak to peak. Immediately after shearing started, the average normal force $F_\perp$ and friction force $F_{//}$ increased to 1.25 mN and 0.6 mN respectively within a few sliding cycles of the upper surface (Figure 2 point a → b). Concomitantly, the separation distance, D, increased significantly upon shearing after the first few sliding cycles and plateaued at $D \approx 75$ nm at time $t \sim 300$ s and increased again monotonically at $t \sim 400$ s (Figure 2 point b→ f). We noticed that this peculiar evolution of D with time was consistent in all the SF tested. A careful observation of the FECO fringes and the contact zone allowed us to categorize the evolution of D in three regimes, denoted as **I**, **II** and **III** (see Figure 3), each corresponding to a different characteristic transformation in the structure of the synovial fluid.

Regime **I** is first characterized by a rapid increase in the separation distance immediately when sliding starts (Figure 2 point a → b, Figure 3A,B). During this rapid increase of D, the surface's shape (assessed by the FECO fringes) reveals a dramatic flattening of the contact area even though the separation distance is increasing. After a few back and forth sliding oscillations, the separation distance measured at the central position of the flat area as well as the shape of the surfaces

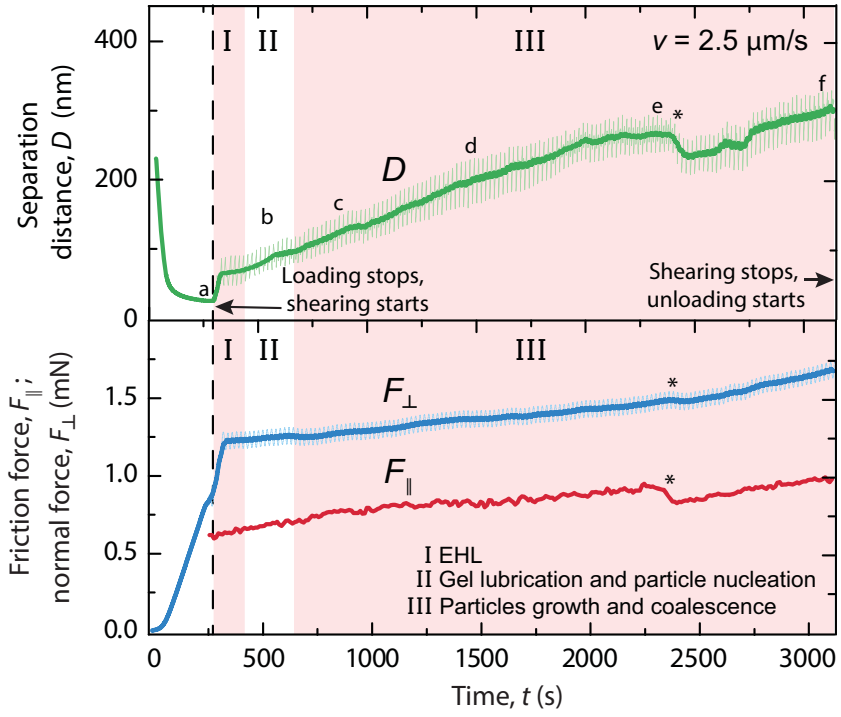

Figure 2. Time evolution of the separation distance, D, normal force, $F_{\perp}$, and friction force, $F_{//}$, between mica surfaces across human synovial fluid. Based on the evolution of D, three regimes were defined as presented on the figure corresponding to different lubrication regimes. Regime I corresponds to elastohydrodynamic lubrication, regime II corresponds to the formation of thick gel layer and regime III involves the formation and rolling of gel particles. Bold lines represent average values during one sliding cycle.

stabilized for a short period. During this short steady state period, the surface's shape showed a characteristic elastohydrodynamic deformation (as observed in the FECO fringes, Figure 3B). As will be shown later, the separation distance between the surfaces presents a wave-like shape indicating that a relaxation process is occurring during each reversal of the sliding direction. The lubrication mechanism in this regime exhibited all of the characteristics of a classical elastohydrodynamic lubrication (EHL) mechanism. In classical EHL, zero slip condition is assumed at the fluid-surface boundary, which gives rise to the characteristic surface deformations observed. These deformations give rise to a normal stress component, which in turn, forces the surface separation to increase. We noticed that the refractive index, n_D, of the fluid at the inlet of the contact, where the pressure is positive, is systematically smaller (but closer to the bulk value of 1.34) than at the outlet, where the pressure is negative. This observation suggests that the fluid entering the contact still possesses the same optical properties as the bulk liquid and then changes when submitted to confined shear. This change in refractive index suggests that denser material is dynamically formed in this region of the contact. Using Multiple Beam Interferometry (MBI), we also confirmed that no significant changes in the birefringence of the sheared film occurred during this regime which suggests that shear induced alignment is not occurring. The time window during which steady state EHL was observed was approximately 100 s for HSF, 200 s for BSF (see Figure SI-3), and increased to 2000 s for ESF (see Figure SI-1).

Regime **II** started when D increased again after the short period of steady state plateau observed at the end of regime **I** (Figure 3C). During this regime, signs of EHL deformations were no longer observed (as visualized by the FECO fringes). The separation distance D between the surfaces slowly increased again and the surfaces slowly adopted a round (undeformed) shape. This regime exhibited all the characteristics of a thick film lubrication regime (TFL) where the bulk rheological properties of the fluid should govern the lubrication properties of the surfaces. Assuming that TFL is effectively present in this regime, we can estimate the effective viscosity of the fluid, η_{eff}, using the following equation:[20]

$$F_{//} = \frac{16}{5}\pi R \eta_{eff} v \log\left(\frac{2R}{D}\right) \text{for} R >> D \quad (3)$$

Using Equation (3) we found that η_{eff} = 105 Pa·s which is 5 orders of magnitude higher than any viscosity value obtained from bulk rheological measurements of synovial fluids at similar shear rates.[21] This apparent discrepancy suggests that the observed lubrication regime is not a true TFL regime in its classical sense.

A careful analysis of the FECO fringes shows that the value of n_D of the confined film was higher than pure synovial fluid and not homogeneous over the entire contact (see arrows pointing to the inhomogeneities in the odd FECO fringes only, in Figure 3C) besides the fact that the film thickness is as high as 140 nm. Moreover, since the surfaces recovered their undeformed shape in this lubrication regime, it is clear that the location of the shear plane has changed from the mica-fluid interface in regime **I** to the bulk of the confined fluid in regime **II**.

Altogether, these observations suggested that a dense film of polyelectrolytes/proteins had formed on the surfaces. The strong anchoring of this film on the mica surfaces had shifted the plane of shear from the mica-fluid interface to the dense film-fluid interface. Moreover, the local variations of n_D observed in the FECO suggested that small particles, denser than the anchored film itself, were gradually forming at the sheared interface (see schematic view regime **II** in Figure 3c). Measurements of the separation distance D after arrest of the surfaces (see Figure SI-7) also showed that the confined film relaxed much faster in this regime than in regime **I**, confirming that its elastic modulus significantly increased. Taken together, these observations demonstrate that this regime is characterized by the formation of an elastic gel layer on the mica surfaces whose thickness increases progressively with shearing time.

Regime **III** started when local deformations of the mica surfaces became evident (Figure 3D). These deformations appeared in both odd and even FECO fringes and were found to systematically

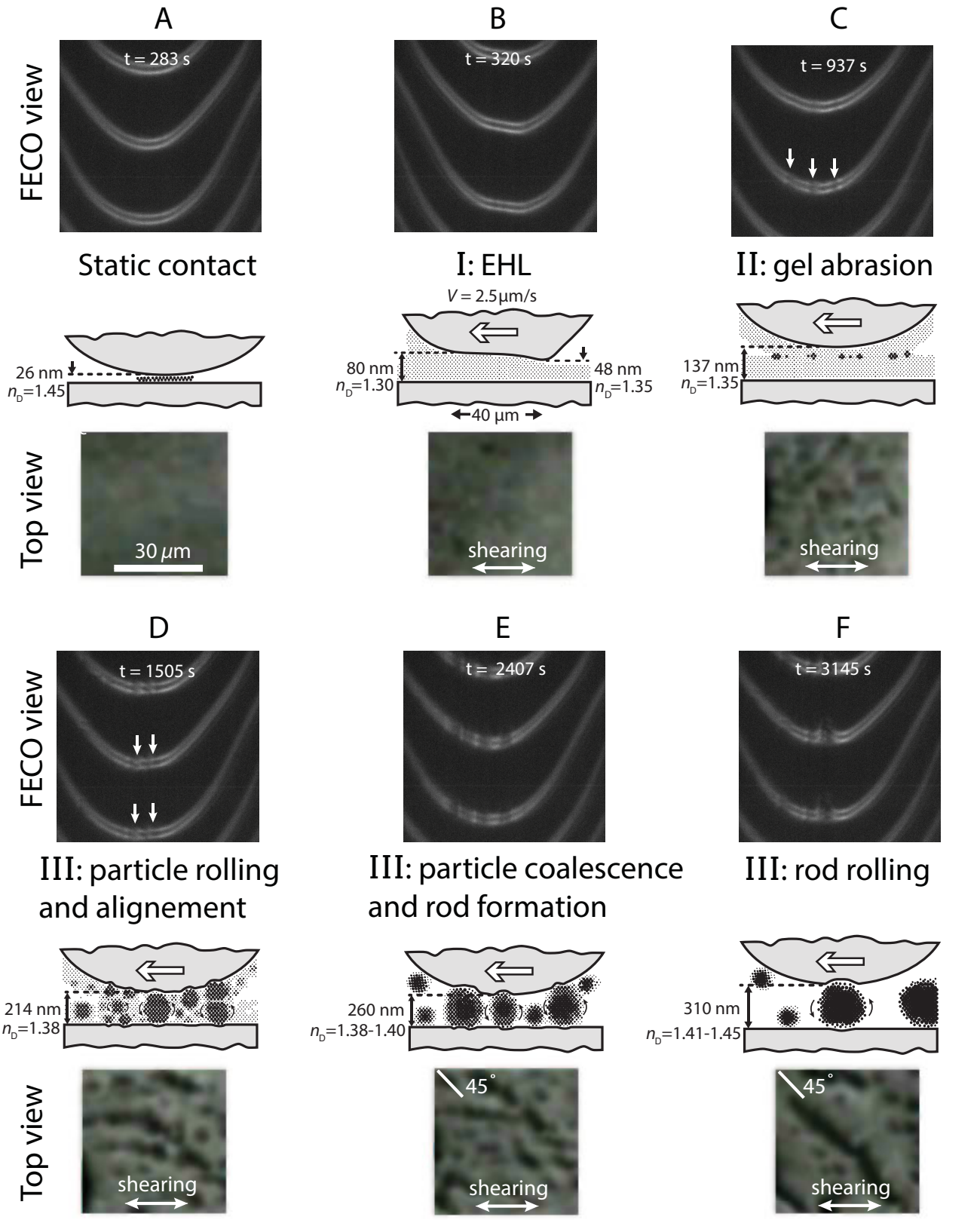

Figure 3. Microstructural changes of human synovial fluid under shear as observed in the FECO fringes and from the top view of the contact. Images A-F corresponds to the points shown in Figure 2. The top view images, obtained by optical microscopy, cover an area similar to the contact area of the surfaces (see also video S1–3 for a larger field of view)

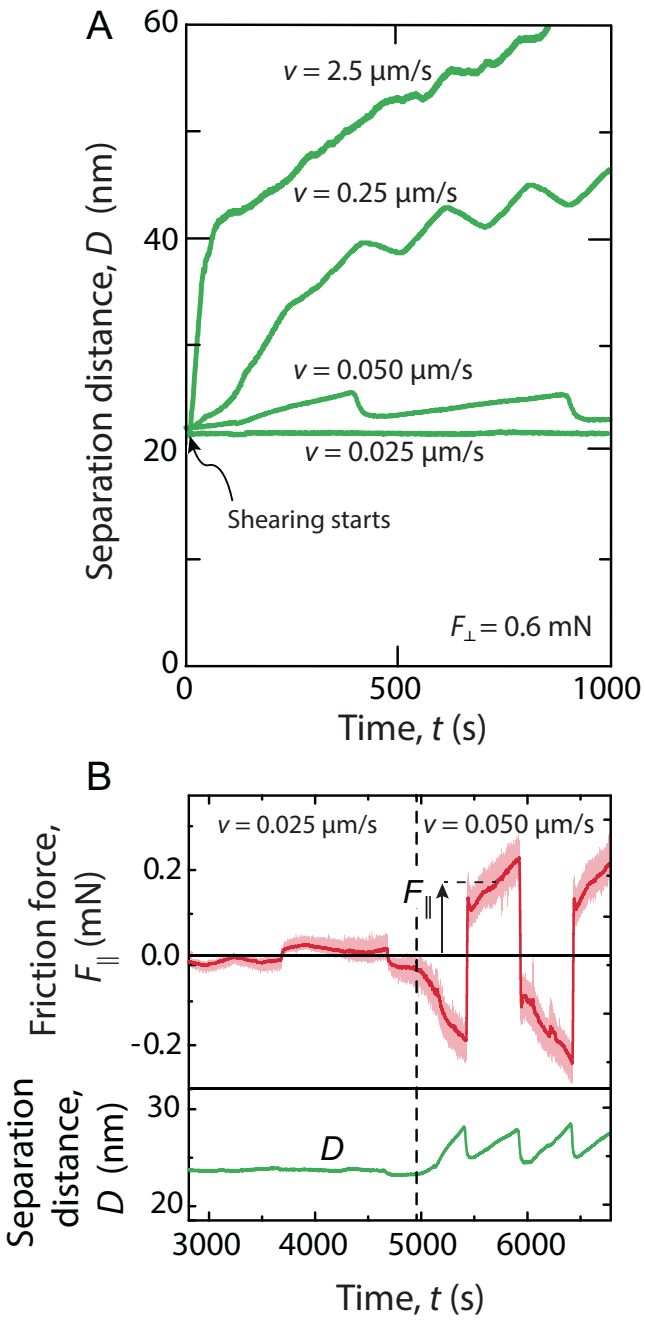

Figure 4. (A) Evolution of the separation distance between two mica surfaces as a function of time under different shearing conditions. At low driving speeds (v = 0.025 µm/s), the separation distance is constant over the whole duration of the experiment. At higher driving speeds (v = 0.050 µm/s), D suddenly exhibits a complex behavior associated to the elastohydrodynamic deformations of the contact but remains constant on average. As the driving is increased again (v > 0.25 µm/s), this complex behavior is replaced by a monotonic increase of D presenting the three characteristic regimes described in Figure 2. (B) Typical changes observed in the friction force and the separation distance when the driving speed is increased from 0.025 µm/s to 0.050 µm/s.

overlap with the deformation induced by variations of n_D. At any deformation points, n_D had a value that was systematically higher than at a non-deformed point and could be as high as 1.45, which was similar to the value measured in a film of thickness of D = 26 nm before shearing. In the undeformed areas of the contact, n_D was found to be close to 1.35, suggesting that dense material was absent in this region and that it was mostly occupied by native SF. The observation of the contact with the normal optical microscope revealed that particles had formed randomly in the sheared area, at least initially (Figure 3C). As they grew, these particles gradually aligned in the shear direction to form "strings of beads" that move at a speed equal to $v/2$ which confirmed that they were rolling between the two surfaces (Figure 3D and video S2). As the particles grew with time, they tended to aggregate laterally with a particle from a close neighbor particle string (Figure 3E). The resulting aggregate had a rod-like shape able to transiently orient its main axis at approximately 45° respective to the shearing direction (Figure 3F, video S3). These aggregates are extremely stable over time (up to 1 h) under drastic dilution conditions (see Figure SI-2), which suggests that this process is mostly irreversible.

This lubrication regime was also marked by large transient variations in D (indicated by a star in Figure 2) which tended to be triggered by the "squeezing out" of a particle from the contact zone. When such an event occurred, D and $F_{||}$ decreased significantly while $F_{\perp}$ decreased only to a smaller extent (indicated with a star in Figure 2).

We noticed that the three regimes just described always appeared in the same chronological order even if their duration changed based on the sliding speed v or the animal species. Importantly, onset of regime **I** systematically triggered the appearance of the other two regimes after a certain time, meaning that regime **I**, **II** and **III** do not represent a stable steady state of the system but are rather transient states. We noticed that the appearance of these transient states is independent of the surface chemistry of the surfaces and, to some extent, to their topography and mechanical properties since the same transformations in the SF were observed between mica surfaces bearing grafted HA molecules (see Figure SI-8).

To further explore the parameters that could affect the duration of each regime, we performed experiments at different sliding speeds, v. As shown in **Figure 4**, at low sliding speed v (typically v < 25 nm/s), the recorded friction trace ($F_{//}$ vs t) showed near horizontal plateaus indicative of smooth sliding between the surfaces. The plateau's position alternated from positive to negative values at each change of sliding direction without any signs of a static friction spike (also known as stiction spike). In this regime, both $F_{\perp}$ and D were found to be constant independent of the shearing time (Figure 4A,B). At higher sliding speeds (typically higher than 50 nm/s), a dramatic increase in the friction force, $F_{//}$, the separation distance, D, and the normal force, $F_{\perp}$ (not shown in Figure 4B), were observed. At such driving speeds, the system started in regime **I** and progressively evolved through regime **II** and **III**. As shown in Figure 4A, oscillations in D with a frequency equal to the driving frequency were clearly observed for v = 50 nm/s and progressively disappeared as the driving velocity was increased.

These observations demonstrate that regime **I**, which corresponds to the EHL regime, is triggered above a critical shear rate, $\dot{\gamma}_c$, which was found to be between 40 and 60 nm/s for all the SF tested at a normal applied force of 0.6–0.75 mN.

Similar observations were made when increasing the normal force at constant driving speed. At a normal force of 5 mN

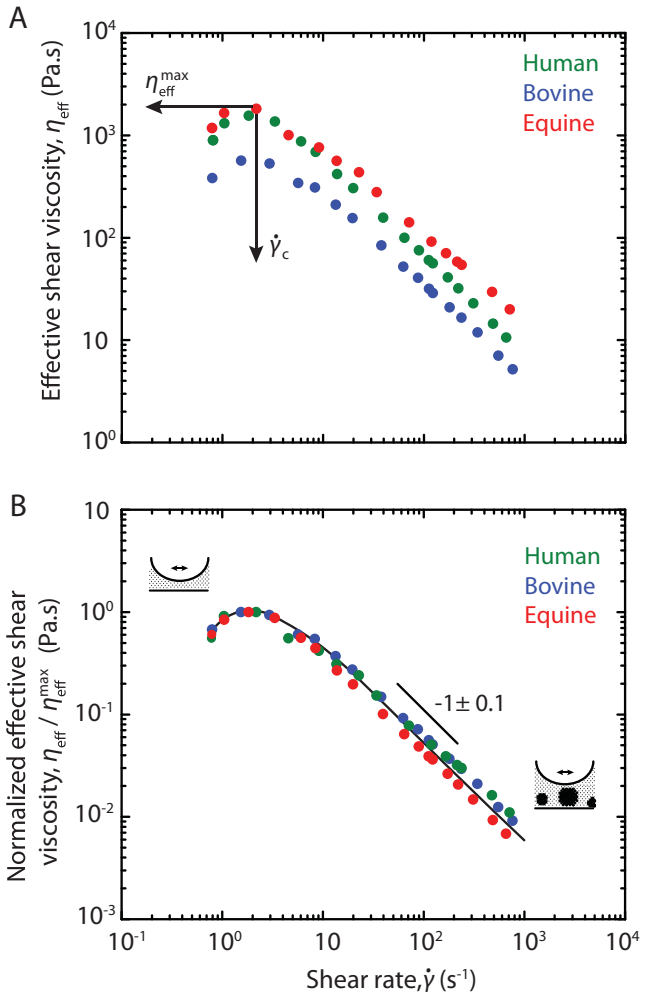

Figure 5. Rheological properties of thin films of synovial fluid. (A) Typical results obtained for the three animal species studied showing a transition from shear thickening at $\dot{\gamma} < \dot{\gamma}_c$ and shear thinning at $\dot{\gamma} > \dot{\gamma}_c$ with a slope of -1. (B) Master curve obtained by normalizing the effective viscosity by the maximum viscosity.

(see Figure SI-5 and 6), the separation distance was found to increase much faster than at 0.8 mN. The FECO fringes also showed that the structural changes of the confined fluid occurred much faster.

The generality of this phenomenon can be appreciated in **Figure 5** where the effective film viscosity, η_{ef} is plotted as a function of the shear rate for the different synovial fluids tested. The results show that the viscosity does not have a simple monotonic dependence with respect to the shear rate but present a maximum at a critical shear rate $\dot{\gamma}_c = v_c/D = 2\ s^{-1}$. At $\dot{\gamma} < \dot{\gamma}_c$, shear thickening of the SF is observed. In this regime, smooth sliding between the surfaces was observed (as in Figure 5B at $v < 0.025$ μm/s) with no hydrodynamic deformations (as seen in the FECO fringes) and no significant variations in D (±1 nm). At $\dot{\gamma} > \dot{\gamma}_c$, clear shear thinning of the fluid was observed. The transition from thickening to thinning corresponds to the transformation from a homogenous fluid layer to a composite fluid film made of native SF and gel particles.

As mentioned before, the formation of the particles and their coalescence is a constantly evolving process, which makes the measurement of properties under steady state, such as the viscosity, a difficult task. In the shear thinning regime, the viscosity of the composite film obeys a simple power law with an exponent of -1. Interestingly, similar exponents have already been reported for confined polymer melts of polybutadiene[22] suggesting that this behavior might be quite general for solutions of high molecular weight polymers.

The molecular origin of the shear thickening and shear thinning regimes is still not clear. The complex and inhomogeneous structure of SF does not allow to fully interpret the rheological transition in terms of transient elastic networks even though certain components of such as HA and Lub are known to interact strongly together. Lubricin, as most mucins, is also known to interact with itself via disulfide bridges. It is therefore natural to envision SF as an effectively highly interconnected network of proteins and polymer chains. Transient networks, such as those formed in associative polymer solutions, are known to exhibit shear thickening-shear thinning transitions in the bulk.[23,24] In these systems, the thickening regime is mainly caused by the stress from the bridge chains highly stretched by shear flow,[23,25] while shear thinning is mostly due to the rupture of the transient network.

Shear thickening of SF could also be due to the formation of strong non covalent bonds between macromolecules and proteins rather than stretching of existing ones. Shear induced formation of complex structures is not uncommon in biological fluids. Shear induced denaturation of proteins and subsequent aggregation has been reported for the formation of long lived amyloid fibrils.[26] The process of blood clotting is known to involve the stretching of von Willebrand factor chains, which expose binding sites to receptors present on the platelets' surface promoting their bridging aggregation.[27] Interestingly, HA macromolecules have been shown to be able to form fibrilar network structures when deposited on mica surfaces[28] and HA solutions have also been shown to form transient structures under low shear rates in bulk solutions,[29] suggesting that HA could be a potential factor of gelation of SF under shear together with previously suggested albumin and γ-globulin[30] and lubricin.[31]

3. Conclusions: Implications of the Findings for Joint Lubrication

Given the independence of our observations on the SF origin and used surface chemistry, we can easily assume that the thickening and particle formation mechanisms observed in this study are also occurring in articular joints and play an essential role in their lubrication.

3.1. Formation Mechanism of the *Lamina Splendens*

The LS of articular surfaces is known to be formed by a thin layer (200–400 nm) of gel like material that can be easily peeled off the cartilage surface.[32] The physical mechanism leading to the formation of this layer is still unknown even

though its composition suggests that it involves SF's main components.[33] The fact that the LS is weakly bound to the cartilage surface strongly suggests that it is mostly formed by SF components from the synovial sac as opposed to SF components from the cartilage micro-pores that could be partially trapped inside the cartilage network and therefore strengthen the bounding between the LS and the superficial zone of the cartilage. Our results suggest that the LS is formed in situ (in the sheared area) from the synovial fluid present in the synovial sac under the action of shear. Our study shows that SF can form a gel layer on cartilage micro asperities under moderate pressures and sliding speeds and that this layer is very stable over time even though it is mechanically fragile. The formation of the LS is therefore a dynamic process, activated locally, where the pressure and the shear rate between the surfaces are the highest, which is essentially where the LS is mostly needed. This mechanism also suggests that the thickness of the LS is not uniform on the cartilage surface and should be thicker in higher stressed regions.

Similar observations on the aggregation behavior of protein solutions have been reported by different research teams using fluids mimicking SF.[34,35] These research groups have shown that mainly seric proteins are directly related to the aggregation behavior of SF mimicking fluids under shear, although recent reports have also shown that lipids might also play an important role.[35] Although it is clear that further studies are necessary to identify which components of the SF are essential to sustain the formation of the LS, previous studies[35] suggest it is a combination of components acting synergistically.

3.2. Role of the *Lamina Splendens* in Cartilage Lubrication

Even though the existence of the LS has been reported for many years, establishing its role in cartilage lubrication remains a challenging task. Several reports have shown that direct removal of the LS either by microtoming or by detergent solubilization[7] does not affect the lubricating properties of cartilage, while other studies using selective digestion or mutant mouse lacking lubricin support the reverse effect.[31,36] These apparent contradictory observations can be reconciled considering the fact that the LS is formed in situ under the action of shear by the confined SF which is not affected by any mechanical or physicochemical removal process (such as microtoming, rubbing or cleaning) but is extremely sensitive to any chemical or genetic degradation process of the SF.

The rather dense structure of the gel layer observed in this study compared to self-adsorbed SF protein films suggests that the LS might also act as a covering membrane of the cartilage surface, maintaining transient fluid pressurization during contact loading and filtrating SF components during exudation and imbibitions of cartilage.

The present SFA study also gives more insight of the role of the LS in the lubrication of articular cartilage. Our results clearly show that the formation of the LS is accompanied by a significant increase in the separation distance between the surfaces and by the appearance of a normal stress component. Increase in the separation distance has clear beneficial effects of keeping the sliding surfaces far apart from direct contact and facilitating the transport of SF in and out of the sheared area. The development of a normal stress component could also promote extra fluid pressurization and flattening of the surface asperities, which also has some beneficial effects on lubrication.

3.3. Synovial Fluid Aggregation and Third Body Lubrication

As we previously mentioned, the shear induced aggregation of protein solutions is a common phenomenon in biological fluids and has recently been observed in different formulations of biomimetic SFs.[9,34,35] The present study suggests that the gel constituting the LS is formed by shear induced aggregation of SF components. The gel is mechanically fragile and can release particles by abrasive wear. The growth mechanism of the particles is similar to a rolling snowball mechanism where the gel and SF continuously adsorb on the particles as they roll.

As mentioned by Murakami et al.,[37] the existence of rolling friction in sheared soft contacts has important implications for joint lubrication as it systematically decreases frictional forces, locally increases the contact pressure promoting SF exudation, and prevents surfaces to come in to close contact even if the LS has been damaged locally.

The formation mechanism of the LS, its lubricating properties, and its interaction with the different components of the SF and cartilage surface, complete the arsenal of previously reported mechanisms of wear protection mechanisms found in articular joints.[38] Each of these mechanisms appears to be efficient under a certain range of shearing conditions, confirming that joint lubrication is an intrinsically adaptive process.[39]

4. Experimental Section

All the experiments performed with each set of fluids were in agreement with the procedures and guidelines provided by the biosafety committee at UCSB.

Synovial Fluids: Human synovial fluid (HSF): Different samples from human donors were collected and tested. Pooled synovial fluid from patients having severe osteoarthritis was obtained from Pr G. Jay from Brown University and was kept frozen before use ($T = -50$ °C). Synovial fluid from healthy donors with no medical record of joint associated diseases was purchased from Cardinal Biological, Inc., Texas USA. The samples were obtained from two female donors of age 72 and 56 years respectively. Bovine synovial fluid (BSF): Pooled synovial fluid from bovine animals was purchased from Animal Technologies, Texas USA. The sample was kept frozen before use. Equine synovial fluid (ESF): Synovial fluid from different horses exhibiting different degrees of osteoarthritis (degree of lameness 1 to 3) was obtained from Alamo Pintado Equine Medical Center, Los Olivos, CA USA.

All fluids were stored at –50 °C before use. In order to avoid freeze-defreeze cycles, aliquots of 4 mL were prepared and discarded after one use. Prior to each experiment, the aliquots were heated at 25 °C and centrifuged in a bench-top centrifuge for 10 min in order to remove any possible cells and tissue debris. After centrifugation, the supernatant fluid was immediately transferred to the surface forces apparatus (SFA).

SFA Surface Preparations: All experiments were performed in an SFA 2000 equipped with a 3D sensor-actuator.[40,41] Surfaces were prepared following previously published standard procedures.[42] Briefly, two back silvered mica surfaces (2–3 μm thick) were glued on cylindrical glass discs using thermosetting glue Epon 1004F. After gluing the mica surfaces, one surface was installed in a glass cup as previously described[43] and transferred to the SFA chamber (lower surface). The other mica surface was installed on the 3D sensor-actuator as previously described[40,41,43] (upper surface). Using Multiple Beam Interferometry, the thickness of the mica surfaces was measured at contact in air.[44] The wavelength of the fringes of equal chromatic order (FECO) were recorded using a CCD camera (Hamamatsu Orca R^2 C10600-10B) and post analyzed using an in-house computer program made with Matlab. After this calibration step, the surfaces were adjusted to a separation distance, D, of 1 mm and the lower cup was then slowly filled with synovial fluid. The bottom of the SFA chamber was filled with water in order to saturate the atmosphere surrounding the surfaces with water vapors and to limit the evaporation of synovial fluid during the course of the experiment. All experiments were performed at 23 °C.

SFA Measurements: Measurements of the normal interaction forces, $F_{\perp}$, were performed using well-established procedures.[40] Briefly, after 1 h of equilibration time, the surfaces were brought close together at a constant approach speed of 0.2 nm/s while simultaneously acquiring the FECO spectra every 0.5 s. Displacement was ensured by a DC motor (Faulhaber) with a 1000:1 gear ratio. The separation distance D between the surfaces and the normal interaction force, $F_{\perp}$, were measured using FECO analysis as previously described.[44] During the experiments, another CCD camera (Pulnix) was also used to image the contact area from the top of the surfaces.[45] The experimental set up allowed for measurement of normal and frictional forces as well as provided FECO and a top view of the contact to be monitored simultaneously in order to detect any changes in surface topography or fluid optical/structural properties.

The 3D sensor actuator uses piezo-actuators controlled by a function generator to generate a reciprocal motion of the upper surface at a constant driving velocity, v. The friction force, $F_{\parallel}$, was detected by semi conductive strain gauges installed on a beam cantilever supporting the upper surface.[40]

Supporting Information

Supporting Information is available from the Wiley Online Library or from the author.

Acknowledgements

This work was supported by the McCutchen Foundation. XB is grateful for the financial support of the Santa Barbara Foundation through the Otis Williams Fellowship. We thank Pr G.D. Jay at Brown University for providing us some of the human synovial fluid samples. Reference 18 was updated on June 4, 2014.

Received: August 23, 2013
Revised: December 1, 2013
Published online: March 2, 2014

[1] a) J. M. Clark, *J. Orthopaed. Res.* **1991**, *9*, 246; b) R. Teshima, T. Otsuka, N. Takasu, N. Yamagata, K. Yamamoto, *J. Bone Joint Surg. Br.* **1995**, *77B*, 460; c) M. J. Kääb, R. G. Richards, P. Walther, I. A. Gwynn, H. P. Nötzli, *Scanning Microscopy* **1999**, *13*.
[2] a) D. Eyre, *Arthritis Res.* **2002**, *4*, 30; b) F. H. Chen, K. T. Rousche, R. S. Tuan, *Nature Clinical Practice Rheumatol.* **2006**, *2*, 373.
[3] R. Crockett, *Tribology Lett.* **2009**, *35*, 77.
[4] B. A. Hills, *P. I. Mech. Eng. H.* **2000**, *214*, 83.
[5] M. Watanabe, C. C. Leng, H. Toriumi, Y. Hamada, N. Akamatsu, S. Ohno, *Med. Electron. Microsc.* **2000**, 33.
[6] a) B. L. Schumacher, J. A. Block, T. M. Schmid, M. B. Aydelotte, K. E. Kuettner, *Arch. Biochem. Biophys.* **1994**, *311*, 144; b) A. R. Jones, J. P. Gleghorn, C. E. Hughes, L. J. Fitz, R. Zollner, S. D. Wainwright, B. Caterson, E. A. Morris, L. J. Bonassar, C. R. Flannery, *J. Orthop. Res.* **2007**, *25*, 283.
[7] a) R. Krishnan, M. Caligaris, R. L. Mauck, C. T. Hung, K. D. Costa, G. A. Ateshian, *Osteoarthr. Cartilage* **2004**, *12*, 947; b) S. Graindorge, W. Ferrandez, E. Ingham, Z. Jin, P. Twigg, J. Fisher, *Proc. Inst. Mech. Eng. H* **2006**, *220*, 597; c) T. Murakami, K. Nakashima, Y. Sawae, N. Sakai, N. Hosoda, *P. I. Mech. Eng. J.-J Eng.* **2009**, *223*, 287.
[8] E. A. Balazs, D. Watson, I. F. Duff, S. Roseman, *Arthritis Rheum.* **1967**, *10*, 357.
[9] K. M. N. Oates, W. E. Krause, R. L. Jones, R. H. Colby, *J. Roy. Soc. Interface* **2006**, *3*, 167.
[10] D. A. Swann, F. H. Silver, H. S. Slayter, W. Stafford, E. Shore, *Biochem. J.* **1985**, *225*, 195.
[11] a) A. V. Sarma, G. L. Powell, M. LaBerge, *J. Orthopaed. Res.* **2001**, *19*, 671; b) B. A. Hills, B. D. Butler, *Ann. Rheum. Dis.* **1984**, *43*, 641.
[12] A. Bensouyad, A. P. Hollander, B. Dularay, A. E. Bedwell, R. A. Cooper, C. W. Hutton, P. A. Dieppe, C. J. Elson, *Ann. Rheum. Dis.* **1990**, *49*, 301.
[13] D. W. Lee, X. Banquy, J. N. Israelachvili, *Proc. Natl. Acad. Sci. USA* **2013**, *110*, E567.
[14] P. G. Degennes, *Adv. Colloid Interface Sci.* **1987**, *27*, 189.
[15] a) M. Benz, N. H. Chen, J. Israelachvili, *J. Biomed. Mater. Res. A* **2004**, *71A*, 6; b) J. Yu, X. Banquy, G. W. Greene, D. D. Lowrey, J. N. Israelachvili, *Langmuir* **2012**, *28*, 2244.
[16] B. Zappone, M. Ruths, G. W. Greene, G. D. Jay, J. N. Israelachvili, *Biophys. J.* **2007**, *92*, 1693.
[17] a) J. Seror, Y. Merkher, N. Kampf, L. Collinson, A. J. Day, A. Maroudas, J. Klein, *Biomacromolecules* **2012**, *13*, 3823; b) J. Seror, Y. Merkher, N. Kampf, L. Collinson, A. J. Day, A. Maroudas, J. Klein, *Biomacromolecules* **2011**, *12*, 3432.
[18] S. Das, X. Banquy, D. W. Lee, G. Greene, B. Zappone, G. Jay, J. Israelachvili, *Biomacromolecules* **2013**, *14*, 1669.
[19] G. D. Jay, J. R. Torres, M. L. Warman, M. C. Laderer, K. S. Breuer, *Proc. Natl. Acad. Sci. USA* **2007**, *104*, 6194.
[20] D. Y. C. Chan, R. G. Horn, *J. Chem. Phys.* **1985**, *83*, 5311.
[21] M. Rinaudo, Y. Rozand, P. Mathieu, T. Conrozier, *Polymers-Basel* **2009**, *1*, 16.
[22] G. Luengo, F. J. Schmitt, R. Hill, J. Israelachvili, *Macromolecules* **1997**, *30*, 2482.
[23] T. Annable, R. Buscall, R. Ettelaie, D. Whittlestone, *J. Rheol.* **1993**, *37*, 695.
[24] R. J. English, H. S. Gulati, R. D. Jenkins, S. A. Khan, *J. Rheol.* **1997**, *41*, 427.
[25] T. Koga, F. Tanaka, *Eur. Phys. J. E* **2005**, *17*, 225.
[26] a) D. E. Dunstan, P. Hamilton-Brown, P. Asimakis, W. Ducker, J. Bertolini, *Protein Engineer. Design Selection* **2009**, *22*, 741; b) D. E. Dunstan, P. Hamilton-Brown, P. Asimakis, W. Ducker, J. Bertolini, *Soft Matter* **2009**, *5*, 5020.
[27] H. Chen, M. A. Fallah, V. Huck, J. I. Angerer, A. J. Reininger, S. W. Schneider, M. F. Schneider, A. Alexander-Katz, *Nat. Commun.* **2013**, *4*, 1333.
[28] M. K. Cowman, C. Spagnoli, D. Kudasheva, M. Li, A. Dyal, S. Kanai, E. A. Balazsy, *Biophys. J.* **2005**, *88*, 590.
[29] A. Maleki, A. L. Kjøniksen, B. Nyström, *Polymer Bull.* **2007**, 59.
[30] J. Y. Fan, C. Myant, R. Underwood, P. Cann, *Faraday Discuss* **2012**, *156*, 69.
[31] G. D. Jay, J. R. Torres, D. K. Rhee, H. J. Helminen, M. M. Hytinnen, C. J. Cha, K. Elsaid, K. S. Kim, Y. J. Cui, M. L. Warman, *Arthritis Rheum.* **2007**, *56*, 3662.
[32] I. C. Clarke, *J. Anat.* **1974**, *118*, 261.
[33] R. Crockett, A. Grubelnik, S. Roos, C. Dora, W. Born, H. Troxler, *J. Biomed. Mater. Res. A* **2007**, *82A*, 958.

[34] a) A. Mavraki, P. M. Cann, *P. I. Mech. Eng. J.-J Eng.* **2009**, *223*, 325; b) K. Nakashima, Y. Sawae, T. Murakami, *Jsme Int. J. C-Mech. Sy.* **2005**, *48*, 555.
[35] D. A. Mirea, A. M. Trunfio-Sfarghiu, C. I. Matei, B. Munteanu, A. Piednoir, J. P. Rieu, M. G. Blanchin, Y. Berthier, *Tribol. Int.* **2013**, *59*, 302.
[36] a) J. M. Coles, L. Zhang, J. J. Blum, M. L. Warman, G. D. Jay, F. Guilak, S. Zauscher, *Arthritis Rheum.* **2010**, *62*, 1666; b) Y. Awae, T. Murakami, K. Matsumoto, M. Horimoto, *Jap. J. Triboloy* **2001**, *45*.
[37] T. Murakami, Y. Sawae, K. Nakashima, S. Yarimitsu, T. Sato, *P. I. Mech. Eng. J.-J Eng.* **2007**, *221*, 237.
[38] a) G. W. Greene, X. Banquy, D. W. Lee, D. D. Lowrey, J. Yu, J. N. Israelachvili, *Proc. Natl. Acad. Sci. USA* **2011**, *108*, 5255; b) T. Murakami, Y. Sawae, M. Ihara, *Jsme Int. J. C-Mech. Sy.* **2003**, *46*, 594.
[39] a) T. Murakami, K. Nakashima, S. Yarimitsu, Y. Sawae, N. Sakai, *P. I. Mech. Eng. J.-J Eng.* **2011**, *225*, 1174; b) T. Murakami, H. Higaki, Y. Sawae, N. Ohtsuki, S. Moriyama, Y. Nakanishi, *P. I. Mech. Eng. H.* **1998**, *212*, 23.
[40] J. Israelachvili, Y. Min, M. Akbulut, A. Alig, G. Carver, W. Greene, K. Kristiansen, E. Meyer, N. Pesika, K. Rosenberg, H. Zeng, *Rep. Progr. Phys.* **2010**, *73*, 036601.
[41] K. Kristiansen, X. Banquy, H. B. Zeng, E. Charrault, S. Giasson, J. Israelachvili, *Adv. Mater.* **2012**, *24*, 5236.
[42] J. N. Israelachvili, N. A. Alcantar, N. Maeda, T. E. Mates, M. Ruths, *Langmuir* **2004**, *20*, 3616.
[43] M. Valtiner, X. Banquy, K. Kristiansen, G. W. Greene, J. N. Israelachvili, *Langmuir* **2012**, *28*, 13080.
[44] J. Israelachvili, *J. Colloid Interf. Sci.* **1973**, *44*, 259.
[45] G. Luengo, M. Tsuchiya, M. Heuberger, J. Israelachvili, *J. Food. Sci.* **1997**, *62*, 767.